Water Splitting

International Edition: DOI: 10.1002/anie.201503407
German Edition: DOI: 10.1002/ange.201503407

NiSe Nanowire Film Supported on Nickel Foam: An Efficient and Stable 3D Bifunctional Electrode for Full Water Splitting**

*Chun Tang, Ningyan Cheng, Zonghua Pu, Wei Xing, and Xuping Sun**

Abstract: *Active and stable electrocatalysts made from earth-abundant elements are key to water splitting for hydrogen production through electrolysis. The growth of NiSe nanowire film on nickel foam (NiSe/NF) in situ by hydrothermal treatment of NF using NaHSe as Se source is presented. When used as a 3D oxygen evolution electrode, the NiSe/NF exhibits high activity with an overpotential of 270 mV required to achieve 20 mA cm^{-2} and strong durability in 1.0 M KOH, and the NiOOH species formed at the NiSe surface serves as the actual catalytic site. The system is also highly efficient for catalyzing the hydrogen evolution reaction in basic media. This bifunctional electrode enables a high-performance alkaline water electrolyzer with 10 mA cm^{-2} at a cell voltage of 1.63 V.*

Hydrogen has been considered as a clean energy resource to replace the diminishing fossil fuel.[1,2] Electrochemical water splitting is a well-established commercial technology to convert electricity produced from intermittent renewable energy resources (such as solar energy, wind, wave power) into chemical energy stored by hydrogen fuel, addressing the issues of effective storage and transport.[3] Although offering an effective way to make high-purity hydrogen, its practical use for mass hydrogen production is limited because it is a strongly uphill reaction with large overpotential (commercial electrolyzers typically operating at a cell voltage of 1.8–2.0 V, which is much higher than the theoretical minimum value of 1.23 V).[4] Active electrocatalysts for anodic oxygen evolution reaction (OER) and cathodic hydrogen evolution reaction (HER) are implemented to overcome the large water-splitting overpotentials, making the process more energy-efficient.[5] Currently, Ir- and Ru-based compounds have the highest activity toward the OER,[6] and platinum group metals are the most efficient HER catalysts,[7] but they suffer from scarcity and high cost, limiting their widespread use. It is thus attractive to design efficient OER and HER catalysts made from earth-abundant elements and, indeed, great progress has been achieved during the past years in developing non-precious metal catalysts with high activity for OER (cobalt phosphate,[8] oxides,[9–12] hydroxides[13–17]) and HER (chalcogenides,[18–21] carbides,[22,23] phosphides[7,24–27]).

Water splitting must be performed in either strongly acidic or alkaline solution to minimize the overpotentials,[28] which however is challenging for earth-abundant catalysts because a high-efficiency catalyst at acidic pH may be inactive or even unstable at alkaline pH and vice versa. Using a bifunctional OER and HER catalyst has advantages of simplifying the system and lowering the cost. Because acidic water splitting suffers from the use of scarce and expensive acid-insoluble OER catalysts with reasonable activity,[29] alkaline water splitting has emerged as a strong candidate for commercialization toward mass hydrogen production.[4] It is thus highly attractive to make a noble-metal-free bifunctional catalyst efficient for both OER and HER in strongly basic media. Grätzel and co-workers have recently reported using NiFe layered double hydroxide on nickel foam (NiFe LDH/NF) as a bifunctional catalyst in alkaline solution, and the water electrolyzer delivers 10 mA cm^{-2} at a cell voltage of 1.7 V, which is much lower than that needed for Ni(OH)$_2$/NF (ca. 1.82 V).[30] We report herein the in situ hydrothermal growth of NiSe nanowires on NF (NiSe/NF) using NaHSe as a Se source. The NiSe/NF as a 3D electrode shows superior catalytic activity and durability for both OER and HER in strongly basic media. The alkaline water electrolyzer in a two-electrode configuration requires a cell voltage of 1.63 V to reach 10 mA cm^{-2}.

Following hydrothermal treatment (see Experimental Section for preparative details), the NF substrate changes to black (Supporting Information, Figure S1). Figure 1 a shows the X-ray diffraction (XRD) pattern. The diffraction peaks at 31.0°, 34.1°, 38.7°, 46.5°, 48.0°, 50.4°, 53.5°, 55.1°, and 56.0° can be indexed to the (300), (021), (211), (131), (410), (401), (321), (330), and (012) planes of NiSe, respectively (JCPDS No. 18-0887).[31] The two peaks at 44.5° and 51.8° arise from NF (JCPDS No. 65-2865). The X-ray photoelectron spectroscopy (XPS) survey spectrum of NiSe/NF shows the characteristic peaks of Ni and Se (Supporting Information, Figure S2 a), and the C 1s and O 1s signals are largely due to contamination/

[*] C. Tang, N. Cheng, Z. Pu, Prof. X. Sun
State Key Laboratory of Electroanalytical Chemistry
Changchun Institute of Applied Chemistry
Chinese Academy of Sciences, Changchun 130022, Jilin (China)
E-mail: sunxp@ciac.ac.cn
N. Cheng
University of the Chinese Academy of Sciences
Beijing 100049 (China)
Prof. X. Sun
Chemistry Department & Center of Excellence for Advanced Materials Research, King Abdulaziz University
Jeddah 21589 (Saudi Arabia)
Prof. W. Xing
Laboratory of Advanced Power Sources
Changchun Institute of Applied Chemistry
Chinese Academy of Sciences, Changchun 130022, Jilin (China)

[**] This work was supported by the National Natural Science Foundation of China (No. 21175129), the National Basic Research Program of China (No. 2011CB935800), and the "Strategic Priority Research Program " of the Chinese Academy of Sciences (No. XDA09030104).

Supporting information for this article is available on the WWW under http://dx.doi.org/10.1002/anie.201503407.

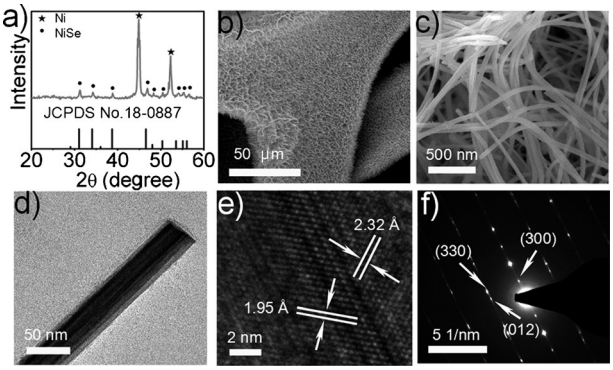

Figure 1. a) XRD pattern of NiSe/NF. b) Low- and c) high-magnification SEM images of NiSe/NF. d) TEM image of one single NiSe nanowire. e) HRTEM image and f) SAED pattern taken from NiSe nanowire.

surface oxidation of the product owing to exposure to atmosphere.[32] The relative intensity of the O 1s peak is large, reflecting a large degree of surface oxidation and the formation of NiO (Supporting Information, Figure S3). The XPS spectra in the Ni 2p, Se 3d, and O 1s regions are shown in the Supporting Information, Figure S2b–d. The Ni $2p_{1/2}$ and Ni $2p_{3/2}$ centered at 873.2 and 855.4 eV correspond to Ni^{II} while the peaks at 852.9 and 870.3 eV can be assigned to metallic Ni 2p arising from the NF substrate[33] (Supporting Information, Figure S2b). In Figure S2c, the peak at 54.3 eV is representative of the Se 3d binding energy, indicating −2 valence of Se and the broad peak near 58.9 eV suggests the surface oxidation state of Se species.[34] The O 1s spectrum also confirms the presence of oxidized Ni due to surface oxidation (Supporting Information, Figure S2d). All these observations support the successful preparation of NiSe with the formation of a nickel oxide layer.[35] Figure 1b shows the low-magnification scanning electron microscopy (SEM) image for NF after selenization, indicating its surface (Supporting Information, Figure S4) is fully covered by densely packed NiSe film. The high-magnification SEM image demonstrates the formation of interconnected NiSe nanowires, usually 20–80 nm in diameter and up to several micrometers in length, as shown in Figure 1c. The energy-dispersive X-ray (EDX) spectrum for the nanowires (Supporting Information, Figure S5) reveals a 1:1.03 Ni:Se ratio, which is consistent within experimental error with the expected 1:1 stoichiometry of NiSe. The transmission electron microscopy (TEM) image further shows such a nanowire has a smooth surface (Figure 1d). The high-resolution TEM (HRTEM) image taken from the nanowire (Figure 1e) displays well-resolved lattice fringes with interplanar distances of 2.32 and 1.95 Å indexed to the (211) and (131) planes of NiSe, respectively. The selected-area electron-diffraction (SAED) pattern (Figure 1f) shows discrete spots indexed to the (300), (330), and (012) planes of the NiSe phase. All of these results strongly support the successful growth of NiSe nanowire film on NF after the hydrothermal process.

We investigated the OER activity of NiSe/NF (NiSe loading: 2.8 mg cm^{-2}) as a 3D electrode in O_2-saturated 1.0 M KOH with a scan rate of 2 mV s^{-1} using a three-electrode configuration. For comparison, similar measurements for bare NF and 20 wt % Pt/C deposited on NF with same loading were also performed. Figure 2a shows their linear sweep voltammetry (LSV) curves on the reversible hydrogen electrode (RHE) scale. Note that all currents presented are corrected against the ohmic potential drop and current densities are based on projected geometric area of an electrode. It is seen that the NiSe/NF electrode exhibits much greater current density and earlier onset of catalytic current compared with bare NF and Pt/C on NF. The oxidation peak at 1.35 V vs RHE observed for NiSe/NF is ascribed to Ni^{II} to Ni^{III}.[36] CV cycling test reveals the oxidation is reversible (Supporting Information, Figure S6). The NiSe/NF requires an overpotential (η_{OER}) of only 270 mV to reach 20 mA cm^{-2}. This η_{OER} is 140 and 50 mV less than that of bare NF and Pt/C on NF, respectively. This value is much lower than that for previously reported $Ni(OH)_2$/NF (ca. 372 mV),[30] $Ni(OH)_2$ (313 mV), and NiO (347 mV) nanoparticles,[37] NiOx/C (335 mV for 10 mA cm^{-2}),[38] NiOOH (525 mV for 10 mA cm^{-2}),[39] amorphous NiO (> 470 mV),[40] $NiCo_2O_4$ (ca. 391 mV),[41] Ni/Ni_3N foam (ca. 399 mV),[42] NiCo LDH (ca. 393 mV),[43] and Ni-Co-O@Ni-Co-S NA (ca. 286 mV),[44] and is even comparable with the behavior of NiFe LDH/NF (ca. 269 mV)[30] and CQDs/NiFe-LDH (ca. 271 mV)[45] in 1.0 M KOH. The OER kinetics is also estimated by corresponding Tafel plots (η versus log(j)) for these electrodes (Figure 2b). The Tafel slope for NiSe/NF is 64 mV dec^{-1}, which is smaller than that of NF (98 mV dec^{-1}) and Pt/C on NF (75 mV dec^{-1}), implying a more rapid OER rate for NiSe/NF electrode. Figure 2c displays a multi-step chronopotentiometric curve for NiSe/NF in 1 M KOH with the current being increased from 50 to 500 mA cm^{-2} (50 mA cm^{-2} per 500 s). The potential immediately levels off at 1.56 V at the start current value and remains unchanged for the rest 500 s, and the other steps also show similar results, implying

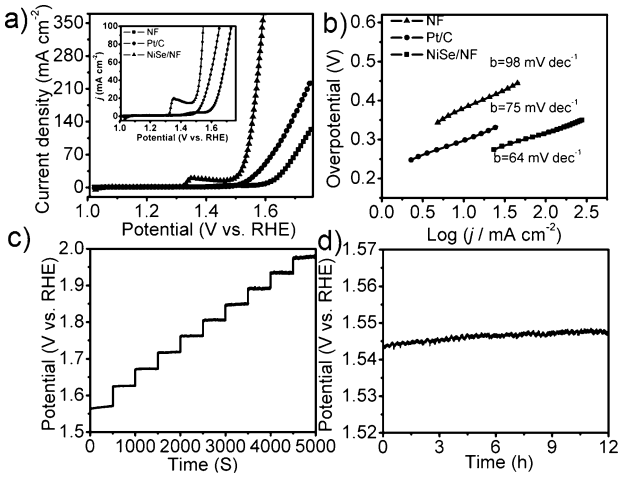

Figure 2. a) LSV curves for NiSe/NF, NF, and Pt/C on NF with a scan rate of 2 mV s^{-1} for OER. b) The corresponding Tafel plots. c) Multi-current process of NiSe/NF. The current density started at 50 mA cm^{-2} and ended at 500 mA cm^{-2}, with an increment of 50 mA cm^{-2} per 500 s without *iR* correction. d) Chronopotentiometric curve of NiSe/NF with constant current density of 100 mA cm^{-2}. All experiments were carried out in 1.0 M KOH.

the excellent mass transportation, conductivity, and mechanical robustness of the 3D NiSe/NF electrode. We further probed the long-term electrochemical stability of this electrode in bulk electrolysis of water in 1.0 M KOH (Figure 2d). As observed, a potential of about 1.544 V is required to deliver 100 mA cm^{-2} and it then stabilizes around this value during the 12 h reaction session. Although vigorous gas evolution occurs during the electrolysis, gas bubbles dissipate rapidly into the solution and no bubbles accumulated on the electrode surface. Although the HRTEM image for the catalyst after OER electrolysis indicates it is still NiSe in nature (Supporting Information, Figure S7), the corresponding Raman spectra analysis (Supporting Information, Figure S8) reveals the formation of NiOOH.[46] It is safe to conclude that the nature of the real catalyst is the active NiOOH formed at the surface.[29,36,47] Indeed, the XPS analysis for the post-OER NiSe/NF demonstrates the formation of Ni^{III} with increased peak intensity of SeO_x (Supporting Information, Figure S9). On the other hand, compared to NF, hydrothermally treated NF needs an η_{OER} of 366 mV to reach 20 mA cm^{-2} with superior activity (Supporting Information, Figure S10) owing to the in situ deposition of active $Ni(OH)_2$ species.[36,48] Note that this NiSe/NF electrode suffers from anodic oxidation dissolution reaction in acidic solution during OER electrolysis, preventing its use in such an environment.

The electrocatalytic HER performances for NiSe/NF, NF, and Pt/C on NF were also assessed in H_2-saturated 1.0 M KOH solution. As shown in Figure 3a, Pt/C on NF needs 40 mV to deliver 10 mA cm^{-2}. Although bare NF is also electroactive toward the HER, the NiSe/NF exhibits much superior activity and requires an overpotential (η_{HER}) of 96 mV to achieve 10 mA cm^{-2}. This overpotential is 159, 53, and 27 mV smaller than that for bare NF, NiS_2/CC,[49] and Ni_3S_2/NF,[50] respectively. Note that this value is 154 and 114 mV less than that for $Ni(OH)_2$/NF and NiFe LDH/NF,[30] respectively, implying the superior HER activity for our NiSe/NF electrode. The CV curve of this potential range shows no redox peaks (Supporting Information, Figure S11), indicating no additional reduction step occurs. The control electrode prepared by scratching down the NiSe catalyst and then immobilizing it on NF using Nafion, $(NiSe/NF)_{Nafion}$, exhibits inferior catalytic activity needing η_{HER} of 187 mV for 10 mA cm^{-2} (Supporting Information, Figure S12). It can be explained as follows: the in situ growth of NiSe on NF for NiSe/NF without using a polymer binder for catalyst immobilization not only enables good mechanical adhesion and electrical connection between them, but also leads to more exposed active sites and improved conductivity.[7,25] Figure 3b presents the corresponding Tafel plots. Pt/C on NF shows a Tafel slope of 43 mV dec^{-1}. The Tafel slope of 120 mV dec^{-1} for NiSe/NF is smaller than bare NF (129 mV dec^{-1}). We also probed the stability of the NiSe/NF electrode by cyclic voltammogram (CV) scan between +0.20 and −0.20 V vs. RHE. The overpotential for achieving 20 mA cm^{-2} only increases by 7 mV after 1000 cycles, as shown in Figure 3c. The long-term electrochemical stability of this electrode was further tested in bulk electrolysis of water. The potential required to deliver 50 mA cm^{-2} is shifted from −0.182 to −0.188 V at the end of 12 h electrolysis (Figure 3d). These results demonstrate the strong stability of NiSe/NF electrode for the HER in 1.0 M KOH. HRTEM image for the post-HER catalyst suggests it still maintains its NiSe nature (Supporting Information, Figure S13). The corresponding XPS spectra show the absence of Ni^{III} and the increase of peak intensity for SeO_x could be attributed to the oxidation of Se at NiSe surface under such strongly alkaline condition (Supporting Information, Figure S14). Furthermore, this NiSe/NF electrode is efficient for the HER with good stability in strongly acidic solution (Supporting Information, Figure S15). Also note that the NiSe/NF is still active for HER and OER after OER and HER electrolysis over 100 CV cycles (Supporting Information, Figure S16).

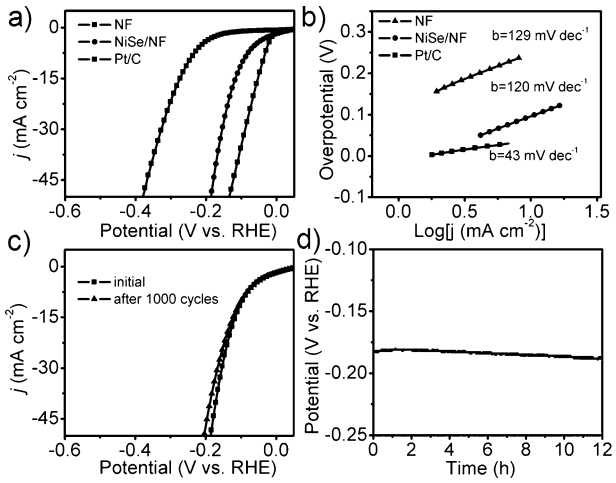

Figure 3. a) LSV curves for NiSe/NF, NF, and Pt/C on NF with a scan rate of 2 mV s^{-1} for HER. b) The corresponding Tafel plots. c) LSV curves for NiSe/NF before and after 1000 CV cycles. d) Chronopotentiometric curve of NiSe/NF with constant current density of 50 mA cm^{-2}. All experiments were carried out in 1.0 M KOH.

Given that NiSe/NF is active and stable catalyst toward both OER and HER in strongly basic media, we made an electrolyzer in a two-electrode setup using NiSe/NF as both anode and cathode to go a step closer to the real application. This alkaline water electrolyzer exhibits high performance with the need of a cell voltage of 1.63 V to afford 10 mA cm^{-2} water-splitting current in 1.0 M KOH (Figure 4a) with vigorous gas evolution on both electrodes (Supporting Information, Figure S17 and Movie S1). This potential compares favorably to the behavior for the electrolyzers based on bare NF (1.93 V), Pt/C on NF (1.67 V), $Ni(OH)_2$/NF (ca. 1.82 V), and NiFe LDH/NF (1.7 V).[30] We also tested the long-term stability of this system for 20 h in 1.0 M KOH. As observed, a potential of 1.75 V is required to deliver 20 mA cm^{-2} at the beginning and stabilizes around 1.74 V after 10 h electrolysis test (Figure 4b). Using our previously reported method,[7,24,25] the generated O_2 and H_2 was further measured quantitatively using a calibrated pressure sensor to monitor the pressure change in the anode and cathode compartment of a H-type electrolytic cell, respectively. The Faradic efficiency (FE) for both processes was calculated by comparing the amount of experimentally quantified gas with theoretically calculated

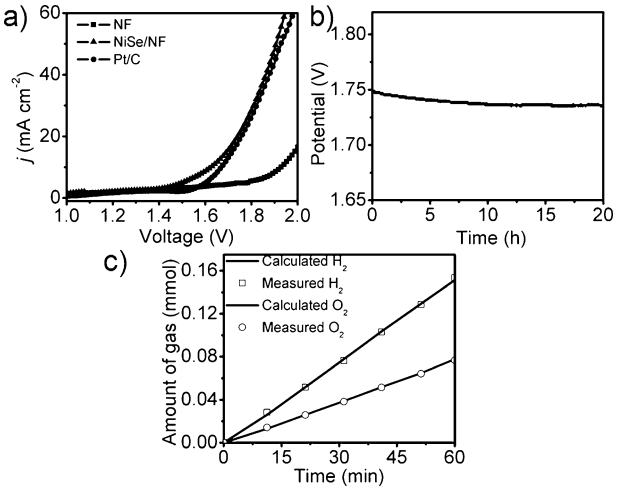

Figure 4. a) LSV curves of water electrolysis for NiSe/NF, NF, and Pt/C on NF in a two-electrode configuration with a scan rate of 2 mV s^{-1}. b) Chronopotentiometric curve water electrolysis for NiSe/NF in a two-electrode configuration with constant current density of 20 mA cm^{-2}. c) The amount of gas theoretically calculated and experimentally measured versus time for overall water splitting of NiSe/NF.

gas (assuming 100% FE). The agreement of both values suggests the FE is 100% for both OER and HER, with the ratio of O_2 and H_2 being close to 1:2 (Figure 4c).

In summary, hydrothermal treatment of NF in the presence of NaHSe has been proven to be a facile strategy for the in situ growth of NiSe nanowires film. The NiSe/NF offers us a novel 3D electrode excellent in activity and durability for OER and HER in strongly alkaline electrolyte. It suggests the NiOOH species formed at the NiSe surface acts as the actual OER catalytic site. We have also demonstrated an efficient water electrolyzer achieving 10 mA cm^{-2} at a cell voltage of 1.63 V with superior stability by applying NiSe/NF as both anode and cathode. The excellent catalytic activity and stability as well as the facile and scale-up fabrication process of this 3D architecture offer promising features for potential use as a noble-metal-free water-splitting electrode in technological devices. This work would also open an exciting new avenue to explore the use of transition-metal selenides toward full water splitting.

Experimental Section

NF was purchased from Shenzhen Green and Creative Environmental Science and Technology Co. Ltd., $NaBH_4$ was bought from Tianjing Fuchen Chemical Reagent Factory. Pt/C (20 wt% Pt on Vulcan XC-72R), Nafion (5 wt%) and Se powder were purchased from Sigma–Aldrich Chemical Reagent Co., Ltd. Hydrochloric acid (HCl) and ethanol were purchased from Aladdin Ltd. (Shanghai, China). All the reagents were used as received. The water used throughout all experiments was purified through a Millipore system.

Preparation of NiSe/NF: A piece of NF (1 × 3 cm^2) was washed with HCl, ethanol and deionized water several times to ensure the surface of the NF was well cleaned before use. For the preparation of NaHSe solution, Se powder (0.059 g) was added into deionized water (1.5 mL) containing $NaBH_4$ (0.065 g). After gentle stirring for several minutes, a clear NaHSe solution was obtained. The freshly prepared NaHSe solution was added into ethanol (30 mL) under N_2 flow. Then the solution was transferred into 50 mL Teflon-lined stainless steel autoclave with a piece of pretreated NF maintained at 140 °C for 12 h in an electric oven. After the autoclave cooled down slowly at room temperature, the sample was collected and washed with water and ethanol several times and then dried at 60 °C for 8 h. The mass of NiSe catalyst on NF was calculated as follows. The weight increment (x mg) of NF can be directly weighted after the growth of NiSe. $NiSe_{loading} = x\ mg \times (M_{NiSe}/M_{Se}) = x\ mg \times (138/79) = 1.7x\ mg$, where M is the molecular weight or atomic weight. For NiSe/NF electrode, the loading mass of NiSe is about 2.8 mg cm^{-2}.

XRD data were acquired on a RigakuD/MAX 2550 diffractometer with Cu K_α radiation ($\lambda = 1.5418$ Å). SEM measurements were carried out on a XL30 ESEM FEG scanning electron microscope at an accelerating voltage of 20 kV. TEM measurements were performed on a HITACHI H-8100 electron microscopy (Hitachi, Tokyo, Japan) with an accelerating voltage of 200 kV. XPS measurements were performed on an ESCALABMK II X-ray photoelectron spectrometer using Mg as the exciting source.

Electrochemical measurements were performed with a CHI 660D electrochemical analyzer (CH Instruments, Inc., Shanghai) in a standard three-electrode system using NiSe/NF as the working electrode, a graphite plate as the counter electrode and an Ag/AgCl electrode as the reference electrode. To prepare the Pt/C loaded electrode, Pt/C (20 mg) and Nafion solution (10 μL 5 wt%) were dispersed in water/ethanol solvent mixture (1 mL, 1:1 v/v) by 30 min sonication to form an ink. Then catalyst ink (140 μL) was loaded on a NF with a catalyst loading of 2.8 mg cm^{-2}. All potentials measured were calibrated to RHE using the following Equation: $E(\mathrm{RHE}) = E(\mathrm{Ag/AgCl}) + 0.197\ \mathrm{V} + 0.059 \times \mathrm{pH}$. All electrolytes were saturated by hydrogen (for HER) and oxygen (for OER) bubbles before and during the experiments. Polarization curves were obtained using LSV with a scan rate of 2 mV s^{-1} and no activation was used before recording the polarization curves. The long-term durability test was performed using chronopotentiometric measurements. All currents presented are corrected against ohmic potential drop.

Keywords: bifunctional catalysts · nanowires · nickel · selenium · water splitting

How to cite: *Angew. Chem. Int. Ed.* **2015**, *54*, 9351–9355
Angew. Chem. **2015**, *127*, 9483–9487

[1] G. W. Crabtree, M. S. Dresselhaus, M. V. Buchanan, *Phys. Today* **2004**, *57*, 39–44.
[2] D. G. Nocera, *Acc. Chem. Res.* **2012**, *45*, 767–776.
[3] J. A. Turner, *Science* **2004**, *305*, 972–974.
[4] K. Zeng, D. Zhang, *Prog. Energy Combust. Sci.* **2010**, *36*, 307–326.
[5] M. G. Walter, E. L. Warren, J. R. McKone, S. W. Boettcher, Q. Mi, E. A. Santori, N. S. Lewis, *Chem. Rev.* **2010**, *110*, 6446–6473.
[6] Y. Lee, J. Suntivich, K. J. May, E. E. Perry, Y. Shao-Horn, *J. Phys. Chem. Lett.* **2012**, *3*, 399–404.
[7] J. Tian, Q. Liu, A. M. Asiri, X. Sun, *J. Am. Chem. Soc.* **2014**, *136*, 7587–7590.
[8] M. W. Kanan, D. G. Nocera, *Science* **2008**, *321*, 1072–1075.
[9] R. D. L. Smith, M. S. Prévot, R. D. Fagan, Z. Zhang, P. A. Sedach, M. K. Siu, S. Trudel, C. P. Berlinguette, *Science* **2013**, *340*, 60–63.
[10] Y. Zhu, W. Zhou, Z. Chen, Y. Chen, C. Su, M. O. Tade, Z. Shao, *Angew. Chem. Int. Ed.* **2015**, *54*, 3897–3910; *Angew. Chem.* **2015**, *127*, 3969–3973.
[11] J. I. Jung, H. Y. Jeong, J. S. Lee, M. G. Kim, J. Cho, *Angew. Chem. Int. Ed.* **2014**, *53*, 4582–4586; *Angew. Chem.* **2014**, *126*, 4670–4674.
[12] T. Ma, S. Dai, M. Jaroniec, S. Qiao, *J. Am. Chem. Soc.* **2014**, *136*, 13925–13931.

[13] F. Song, X. Hu, *J. Am. Chem. Soc.* **2014**, *136*, 16481 – 16484.
[14] X. Long, J. Li, S. Xiao, K. Yan, Z. Wang, H. Chen, S. Yang, *Angew. Chem. Int. Ed.* **2014**, *53*, 7584 – 7588; *Angew. Chem.* **2014**, *126*, 7714 – 7718.
[15] S. Chen, J. Duan, M. Jaroniec, S. Qiao, *Angew. Chem. Int. Ed.* **2013**, *52*, 13567 – 13570; *Angew. Chem.* **2013**, *125*, 13812 – 13815.
[16] W. D. Chemelewski, H.-C. Lee, J.-F. Lin, A. J. Bard, C. B. Mullins, *J. Am. Chem. Soc.* **2014**, *136*, 2843 – 2850.
[17] L. Trotochaud, S. L. Young, J. K. Ranney, S. W. Boettcher, *J. Am. Chem. Soc.* **2014**, *136*, 6744 – 6753.
[18] Y. Xu, M. Gao, Y. Zheng, J. Jiang, S. Yu, *Angew. Chem. Int. Ed.* **2013**, *52*, 8546 – 8550; *Angew. Chem.* **2013**, *125*, 8708 – 8712.
[19] J. Yang, D. Voiry, S. J. Ahn, D. Kang, A. Y. Kim, M. Chhowalla, H. S. Shin, *Angew. Chem. Int. Ed.* **2013**, *52*, 13751 – 13754; *Angew. Chem.* **2013**, *125*, 13996 – 13999.
[20] C. G. Morales-Guio, X. Hu, *Acc. Chem. Res.* **2014**, *47*, 2671 – 2681.
[21] D. Kong, H. Wang, Z. Lu, Y. Cui, *J. Am. Chem. Soc.* **2014**, *136*, 4897 – 4900.
[22] W. Cui, N. Cheng, Q. Liu, C. Ge, A. M. Asiri, X. Sun, *ACS Catal.* **2014**, *4*, 2658 – 2661.
[23] L. Liao, S. Wang, J. Xiao, X. Bian, Y. Zhang, M. D. Scanlon, X. Hu, Y. Tang, B. Liu, H. H. Girault, *Energy Environ. Sci.* **2014**, *7*, 387 – 392.
[24] Q. Liu, J. Tian, A. M. Asiri, X. Sun, *Angew. Chem. Int. Ed.* **2014**, *53*, 6710 – 6714; *Angew. Chem.* **2014**, *126*, 6828 – 6832.
[25] P. Jiang, Q. Liu, Y. Liang, J. Tian, A. M. Asiri, X. Sun, *Angew. Chem. Int. Ed.* **2014**, *53*, 12855 – 12859; *Angew. Chem.* **2014**, *126*, 13069 – 13073.
[26] E. J. Popczun, J. R. McKone, C. G. Read, A. J. Biacchi, A. M. Wiltrout, N. S. Lewis, R. E. Schaak, *J. Am. Chem. Soc.* **2013**, *135*, 9267 – 9270.
[27] E. J. Popczun, C. G. Read, C. W. Roske, N. S. Lewis, R. E. Schaak, *Angew. Chem. Int. Ed.* **2014**, *53*, 5427 – 5430; *Angew. Chem.* **2014**, *126*, 5531 – 5534.
[28] E. A. Hernández-Pagán, N. M. Vargas-Barbosa, T. H. Wang, Y. Zhao, E. S. Smotkin, T. E. Mallouk, *Energy Environ. Sci.* **2012**, *5*, 7582 – 7589.
[29] M. S. Burke, M. G. Kast, L. Trotochaud, A. M. Smith, S. W. Boettcher, *J. Am. Chem. Soc.* **2015**, *137*, 3638 – 3648.
[30] J. Luo, J.-H. Im, M. T. Mayer, M. Schreier, M. K. Nazeeruddin, N. G. Park, S. D. Tilley, H. Fan, M. Grätzel, *Science* **2014**, *345*, 1593 – 1596.
[31] L. Mi, H. Sun, Q. Ding, W. Chen, C. Liu, H. Hou, Z. Zheng, C. Shen, *Dalton Trans.* **2012**, *41*, 12595 – 12600.
[32] A. Panneerselvam, M. A. Malik, M. Afzaal, P. O'Brien, M. Helliwell, *J. Am. Chem. Soc.* **2008**, *130*, 2420 – 2421.
[33] P. Prieto, V. Nistor, K. Nouneh, M. Oyama, M. Abd-lefdil, R. Díaz, *Appl. Surf. Sci.* **2012**, *258*, 8807 – 8813.
[34] S. Huang, Q. He, W. Chen, Q. Qiao, J. Zai, X. Qian, *Chem. Eur. J.* **2015**, *21*, 4085 – 4091.
[35] X. Yu, W. Sun, Y. Chu, *New J. Chem.* **2014**, *38*, 70 – 76.
[36] M. W. Louie, A. T. Bell, *J. Am. Chem. Soc.* **2013**, *135*, 12329 – 12337.
[37] L.-A. Stern, X. Hu, *Faraday Discuss.* **2014**, *176*, 363 – 379.
[38] Y. Qiu, L. Xin, W. Li, *Langmuir* **2014**, *30*, 7893 – 7901.
[39] S. Klaus, Y. Cai, M. W. Louie, L. Trotochaud, A. T. Bell, *J. Phys. Chem. C* **2015**, *119*, 7243 – 7254.
[40] L. Kuai, J. Geng, C. Chen, E. Kan, Y. Liu, Q. Wang, B. Geng, *Angew. Chem. Int. Ed.* **2014**, *53*, 7547 – 7551; *Angew. Chem.* **2014**, *126*, 7677 – 7681.
[41] Z. Peng, D. Jia, A. M. Al-Enizi, A. A. Elzatahry, G. Zheng, *Adv. Energy Mater.* DOI: 10.1002/aenm.201402031.
[42] M. Shalom, D. Ressing, X. Yang, G. Clavel, T. P. Fellinger, M. Antonietti, *J. Mater. Chem. A* **2015**, *3*, 8171 – 8177.
[43] H. Liang, F. Meng, M. Cabán-Acevedo, L. Li, A. Forticaux, L. Xiu, Z. Wang, S. Jin, *Nano Lett.* **2015**, *15*, 1421 – 1427.
[44] W. Xu, Z. Lu, X. Lei, Y. Li, X. Sun, *Phys. Chem. Chem. Phys.* **2014**, *16*, 20402 – 20405.
[45] D. Tang, J. Liu, X. Wu, R. Liu, X. Han, Y. Han, H. Huang, Y. Liu, Z. Kang, *ACS Appl. Mater. Interfaces* **2014**, *6*, 7918 – 7925.
[46] K. S. Joya, X. Salac, *Phys. Chem. Chem. Phys.* DOI: 10.1039/c4cp05053c.
[47] W. Zhou, X. Wu, X. Cao, X. Huang, C. Tan, J. Tian, H. Liu, J. Wang, H. Zhang, *Energy Environ. Sci.* **2013**, *6*, 2921 – 2924.
[48] J. Tian, Z. Xing, Q. Chu, Q. Liu, A. M. Asiri, A. H. Qusti, A. O. Al-Youbi, X. Sun, *CrystEngComm* **2013**, *15*, 8300 – 8305.
[49] C. Tang, Z. Pu, Q. Liu, A. M. Asiri, X. Sun, *Electrochim. Acta* **2015**, *153*, 508 – 514.
[50] C. Tang, Z. Pu, Q. Liu, A. M. Asiri, Y. Luo, X. Sun, *Int. J. Hydrogen Energy* **2015**, *40*, 4727 – 4732.

Received: April 15, 2015
Revised: June 8, 2015
Published online: July 1, 2015

